Statistics of wave functions in disordered systems with applications to Coulomb blockade peak spacing

Mike Miller, Denis Ullmo,* and Harold U. Baranger
Department of Physics, Duke University, Durham, North Carolina 27708-0305, USA
(Received 21 June 2004; revised manuscript received 2 March 2005; published 5 July 2005)

Despite considerable work on the energy-level and wave function statistics of disordered quantum systems, numerical studies of those statistics relevant for electron-electron interactions in mesoscopic systems have been lacking. We plug this gap by using a tight-binding model to study a wide variety of statistics for the two-dimensional, disordered quantum system in the diffusive regime. Our results are in good agreement with random matrix theory (or its extensions) for simple statistics such as the probability distribution of energy levels or spatial correlation of a wave function. However, we see substantial *disagreement* in several statistics which involve both integrating over space and different energy levels, indicating that disordered systems are more complex than previously thought. These are exactly the quantities relevant to electron-electron interaction effects in quantum dots; in fact, we apply these results to the Coulomb blockade, where we find altered spacings between conductance peaks and wider spin distributions than traditionally expected.

DOI: 10.1103/PhysRevB.72.045305 PACS number(s): 73.21.−b, 72.15.Rn, 73.23.Hk, 05.45.Mt

I. INTRODUCTION

The interplay between electron-electron interactions and quantum interference has been a theme in condensed matter physics for the last two decades.[1–4] The classic context is interaction effects in disordered systems.[1,2] More recently, mesoscopic systems, such as quantum dots[3] or metallic nanoparticles,[4] have been intensively investigated; both diffusive disordered and ballistic chaotic systems have received attention.

A key quantity in studying such effects is the statistics of the single-particle wave functions as one moves from level to level, system to system, or in position space. It is well established that weakly disordered quantum systems, as well as ballistic chaotic ones, display universal statistical behavior.[5–8] Universal here means that the properties do not depend on the microscopic details of the disorder, such as its spatial correlation function. As the behavior is universal, it can be captured by relatively simple models. In fact, many properties are described well by random matrix theory (RMT); for those which involve the spatial behavior of wave functions, a simple extension of RMT in which eigenstates are described as a superposition of random plane waves (RPW) is accurate.[5–8] In both computational and experimental results, for instance, the probability distribution of the spacing between adjacent energy levels and the magnitude of the wave function at a single point closely match RMT predictions.[9–16] Complications arise as disorder increases and the wave functions become increasingly nonuniform spatially. Such systems have been investigated extensively, including localized systems[17–19] with wave functions confined to a small area of the system. Diffusive systems of intermediate disorder values are of the greatest interest to mesoscopic physics; complexities due to incipient localization effects have also been studied there.[20,21]

Despite this recent interest, several of the eigenfunction statistics most relevant to problems in mesoscopic physics have never, as far as we know, been studied. The interaction contribution to the energy, for instance, involves sums over different energy levels of matrix elements of the residual (screened) interaction, each of which involves an integration over space. Here we particularly study statistics involving *both* different energies and integration over space. We find that these statistics deviate strongly from expectations, indicating that disordered systems are more complex than previously thought. We include an analysis of how these results fit with previous experimental and theoretical results, including calculations from the supersymmetric σ model.[16,21] We then apply our statistics to the Coulomb blockade problem. Parameters of the study have been chosen for the greatest relevance to the physical conditions of the Coulomb blockade in semiconductor quantum dots.

We wish to emphasize that the issue here is *not* the existence of a new regime of behavior but rather *new characteristics* in a regime that has been intensively studied for three decades. To make this point, it is necessary to demonstrate beyond a shadow of a doubt that our calculations are performed in the familiar regime of parameters. Thus, after explaining our methodology in Sec. II, we establish in Sec. III, for simple eigenfunction statistics, a general agreement with previous results. The comparison with previous work is by no means exhaustive but rather serves to confirm the diffusive nature of our system and to demonstrate that we get agreement with RMT/RPW expectations for these well-researched statistics. The core of our paper lies in Sec. IV, where we introduce energy correlation statistics that depart markedly from current analytical predictions, thus demonstrating surprising complexities underlying the disordered model, even for parameters that generate agreement with the simple statistics investigated in Sec. III. The key numerical results are in Figs. 12 and 13. Section V contains a detailed comparison between our numerical results and the existing analytic results obtained by the supersymmetric σ model and RMT/RPW methods. Finally, we explore the importance of these energy correlation statistics in Sec. VI, where the new results are directly applied to the Coulomb blockade.

II. METHODOLOGY

All results in this paper were derived within the Anderson model, a standard model for describing disordered systems.[17] The Anderson model employs a discrete lattice geometry, and combines a "hopping" Hamiltonian with a set of uncorrelated on-site energies

$$\hat{H} = \sum_i |i\rangle \epsilon_i \langle i| - V \sum_i (|i\rangle\langle i+1| + |i-1\rangle\langle i|). \quad (1)$$

In more than one dimension, the hopping component includes transitions to all nearest neighbors. For simplicity, we take V, the transition amplitude, and a, the lattice spacing, both equal to 1. The ϵ_i's are uncorrelated from site to site, and ϵ_i/V are drawn from a uniform random distribution of width W, which measures the disorder strength of the system. To treat a magnetic field, the appropriate phase factor can be added to V.[22,23] Our study concentrates on a two-dimensional rectangle of size 164×264 with hard-wall boundaries. The large size allows us to choose parameters such that the disorder is weak but the mean free path is less than the system size; hard wall boundary conditions are more appropriate for realistic quantum dots than other simple possibilities; and the asymmetry breaks pseudodegeneracies in the eigenband. Some characteristics of other geometries, such as smaller systems or periodic boundary conditions (corresponding to a torus), are touched on where appropriate.

Three main variables can be adjusted to control the physical regime: (i) the mean energy around which to draw statistics, (ii) the disorder strength, and (iii) the strength of any applied magnetic field.

First, each fully diagonalized matrix in this study would produce 164×264 eigenfunctions. Because of the large size, computing constraints made it reasonable to analyze only eigenfunctions within a narrow band of eigenenergies, here expressed in terms of a "filling ratio." This ratio indicates the position of the chosen band's central eigenfunction in the full eigenenergy band. The presented statistics are averaged over both the band's many eigenfunctions and separate disorder realizations. We analyze energy bands centered at 1/25 and 1/100 filling, with band width about 1/100. The very low energy in the second case was chosen to match physical quantum dots, which typically contain only hundreds of electrons. As an added benefit, low energies result in a larger wavelength ($k_F a = 0.72$ and 0.35, so that $\lambda_F \approx 9a$ and $18a$, respectively), compensating for the somewhat arbitrary nature of a discrete geometry.

Second, the disorder strength of the system, measured as W, has a profound effect on the system's behavior. Our results will first demonstrate trends as W is varied, and then focus on specific W values. Very small W produces a semiballistic system, whereas very large W produces localized eigenfunctions. We are most interested in intermediate disorder, which yields a diffusive system.

Finally, we are also interested in the effect of a small magnetic field, enough to break time reversal invariance but not enough to cause well-defined Landau levels, for instance. To add a magnetic field B' perpendicular to the system plane, we adjust the hopping amplitude in the Hamiltonian by using the Peirels substitution[22,23]

$$\psi(r) \Rightarrow e^{i2\pi \int A' dl/\varphi_0} \psi(r), \quad A' = B' y \hat{x}. \quad (2)$$

This implies that one changes the hopping terms in the x direction according to

$$-1 \Rightarrow -e^{\pm i2\pi B' y a/\varphi_0} \Rightarrow -e^{\pm i y a B/\mathcal{A}}, \quad (3)$$

where a is the lattice constant, $\mathcal{A}$ is the area of the system ($\mathcal{A}/a^2$ is the number of lattice sites), and B is the magnetic field in units of magnetic flux quanta through 2π times the area of the system.

We analyze below both the $B=0$ case and a system with sufficient magnetic field to break time-reversal invariance. By analyzing trends as a function of B, we determined that $B=6$ is sufficient. The results in the presence of a magnetic field are applied to the Coulomb blockade problem.

III. SIMPLE STATISTICS: AGREEMENT WITH RMT/RPW

Before delving into relatively unexplored statistics, we want to first determine the parameters corresponding to the diffusive regime and confirm that, for simple eigenfunction statistics, our computations match previous analytical and numerical work. We do not carry out a comprehensive comparison with past results but rather present enough to convincingly show that RMT augmented by RPW or perturbative techniques accounts for these properties, all as a prelude to the striking disagreement presented in the next section. For simplicity, we start with $B=0$ and study only eigenfunctions in the low-energy range most relevant to mesoscopic physics.

We begin by establishing the disorder strength W corresponding to diffusivity. To do this, we consider the inverse participation ratio (IPR)

$$\mathrm{IPR} = \mathcal{A} \int |\psi(\mathbf{r})|^4 d^2 r. \quad (4)$$

$\mathcal{A}$ is the area of the system, and we understand the integral to be taken as a discrete sum over lattice sites. The IPR is closely linked to the degree of localization within the system,[24] and is inversely proportional to the volume in which the wave function is confined. Large IPR values thus correspond to strongly localized states. It can be derived from basic RMT that the IPR for a time-reversal invariant system should have a universal mean value of 3.0, with small variations from this mean.[25,26] Chaotic systems, and weakly disordered experimental systems, do show a mean of 3.0, with a nearly symmetrical distribution around this value.[14,27,28] The mean IPR obtained by averaging over disorder realizations has been extensively studied numerically for both two- and three-dimensional systems.[29–32] The expectation is that the IPR should remain roughly constant for disorder values in the diffusive regime, and then should rise sharply for greater disorder values in the localized regime.

Figure 1 shows our results for the variation of $\langle \mathrm{IPR} \rangle$ against disorder strength for both 1/25 and 1/100 filling. Note three important features: IPR is consistently higher for

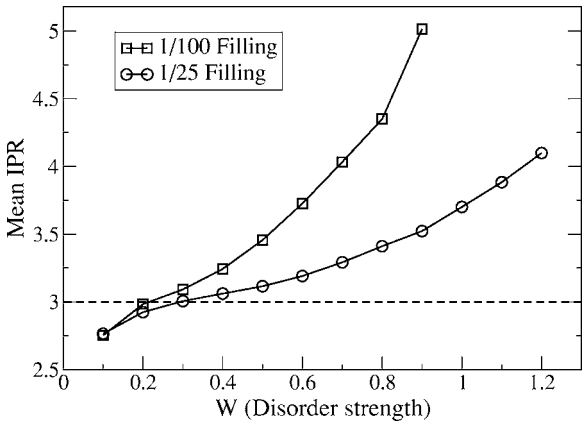

FIG. 1. The mean inverse participation ratio (IPR) as a function of disorder for two energies. The mean IPR increases with disorder; the plateau in the middle of each curve, most noticeable for 1/25 filling, corresponds to the diffusive regime. RMT predicts a universal value of 3.0 (dotted line). The system is a 164×264 rectangle, at $B=0$, with five disorder realizations and about 400 different states used in each case.

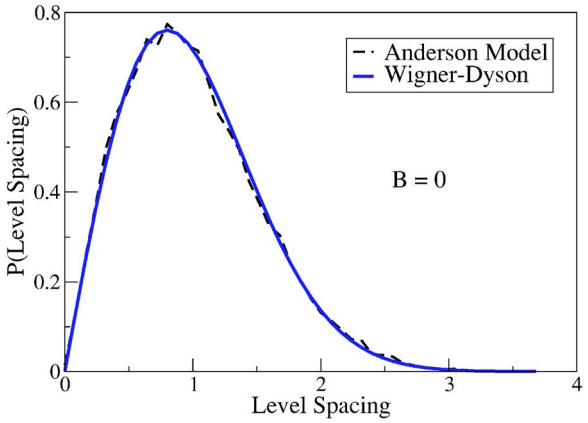

FIG. 2. (Color online) Probability density of the spacing between neighboring energy levels. The calculated distribution (dashed) matches the Wigner surmise (solid) obtained from the orthogonal ensemble of RMT. Both the mean and integral are normalized to 1. (Filling is 1/25 and $B=0$.)

the lower energy band, IPR rises with disorder strength, and the pattern of this trend suggests three separate regimes of behavior. Between $W=0.1$ and 0.3, we see a saturating increase in both graphs; between $W=0.3$ and 0.5, we see a linear trend, especially in the 1/25 case; and for higher W values, we see rapidly increasing behavior. It is reasonable to expect these three statistically distinct regimes to correspond, at least roughly, to the three physically relevant regimes: semiballistic, diffusive, and localized. Figure 1 thus suggests we can choose $W=0.2$, 0.5 and 0.8 or higher as representative values of these three regimes in the 1/25 filling case.

For further verification that these disorder values correspond to the diffusive regime, we find the three characteristic length scales for our system: the electron wavelength, the mean free path l and the localization length L_{loc}. By comparing the size of the system L to these three lengths, the various regimes are defined. In the diffusive regime one expects

$$\lambda_F \ll l \ll L \ll L_{\mathrm{loc}}. \tag{5}$$

In the semiballistic regime, the system size is smaller than the mean free path, while in the localized regime, the localization length is smaller than the system size.

According to calculations using the Born approximation,[33] at 1/25 filling, $l/a=24/W^2$, and at 1/100 filling, $l/a=11.5/W^2$. For L, we take the small side of the rectangle, $L=164a$. On the other hand, it is known that $L_{\mathrm{loc}}=cN_{\mathrm{ch}}l$, where c is a constant found to be about 2. N_{ch}, the number of transverse channels in the system, is based solely on the energy of the system, and is given by $N_{\mathrm{ch}}=k_FL/\pi$. At 1/25 filling, $N_{\mathrm{ch}}=37$; at 1/100 filling, $N_{\mathrm{ch}}=18$. We can thus calculate, for the two energy levels, the required W values for a diffusive regime

$$1/25 \text{ filling}: 24/W^2 \ll 164 \ll 1800/W^2 \Rightarrow 0.38 \ll W \ll 3.3, \tag{6}$$

$$1/100 \text{ filling}: 11.5/W^2 \ll 164 \ll 420/W^2 \Rightarrow 0.26 \ll W \ll 1.6. \tag{7}$$

This confirms the choice of $W=0.5$ for 1/25 filling as belonging in the diffusive regime ($\lambda_F=9a, l=96a, L_{\mathrm{loc}}=7200a$), and prompts the choice of $W=0.35$ for 1/100 filling ($\lambda_F=18a, l=94a, L_{\mathrm{loc}}=3400a$).

We can now begin to look at some of the basic statistics of our diffusive system and compare them to RMT prediction and experiment. For clarity, we will present only the 1/25 filling results in the zero magnetic field case to establish general agreement, and then proceed to the lower energy when we add a magnetic field and begin to concentrate on the energy correlation statistics relevant to the Coulomb blockade problem.

One of the simplest and most comprehensively studied statistics is the distribution of the spacing between adjacent energy levels, $P(s)$.[7] A basic result of RMT is that $P(s)$ is very well approximated by the classic Wigner surmise, given in the absence of a magnetic field by

$$P(s) = \frac{\pi}{2} s e^{-\pi s^2/4}. \tag{8}$$

Figure 2 compares this prediction with our calculated energy spacing distribution. We see excellent agreement on all parts of the graph; the match is equally good for 1/100 filling, not shown here.

Another well-studied statistic is the magnitude of the wave function at a single point. In the absence of a magnetic field, it is expected to follow the classic Porter-Thomas distribution[34]

$$P(t) = \frac{1}{\sqrt{2\pi t}} e^{-t/2}, \quad t = |\psi(r)|^2 \mathcal{A}. \tag{9}$$

Both ballistic chaotic and weakly disordered systems show this behavior.[10–15,26,35] The predicted IPR value of 3.0 is derived by taking the appropriate moment of this Porter-

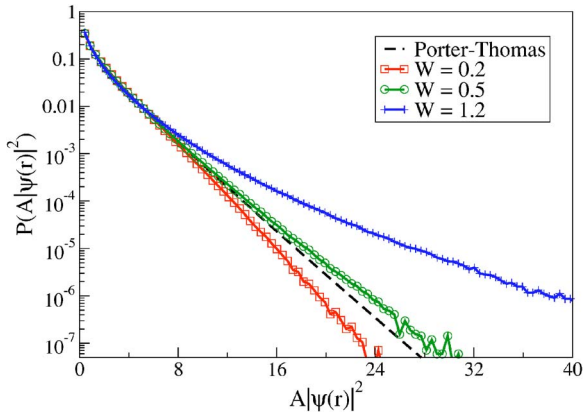

FIG. 3. (Color online) Probability distribution of $\mathcal{A}|\psi(\mathbf{r})|^2$ in three different regimes: semi-ballistic at $W=0.2$ (squares), diffusive at $W=0.5$ (circles), and localized at $W=1.2$ (pluses). In the diffusive case, we see excellent agreement with the Porter-Thomas distribution predicted by RMT. The integral of each curve is normalized to 1. Filling is 1/25 and $B=0$. (Because of the hard-wall boundary condition, the probabilities were sampled on the inner 3/4 of the rectangle.)

Thomas result. Note the general RMT prediction of approximately uniformly extended wave functions (in position space) such that large wave function amplitudes are exponentially rare.

Figure 3 displays our results for the probability distribution of $|\psi(r)|^2$ in the three different regimes. We see excellent agreement across the graph for the diffusive case, another indication that this system is truly diffusive. As we can see from the figure, the higher the disorder value W, the greater the prevalence of both very large and very small $|\psi(r)|^2$ values, indicating the system is becoming more localized and less uniform.

To transition to system-wide eigenfunction characteristics, we first look at the spatial correlation statistic, the correlation between sites separated by a certain distance

$$\psi \text{ correlation} = \mathcal{A}\langle\psi(\mathbf{r})\psi(\mathbf{r}+\mathbf{r}')\rangle, \tag{10}$$

$$\psi^2 \text{ correlation} = \mathcal{A}^2\langle\psi^2(\mathbf{r})\psi^2(\mathbf{r}+\mathbf{r}')\rangle. \tag{11}$$

Notice that the IPR is the value of the second correlation function at $\mathbf{r}'=0$. RMT gives an overly simple prediction for these correlations: All off-diagonal terms are equivalent and have a value consistent with normalization of the wave function. A much more useful prediction can be obtained from Berry's idea that a wave function of a chaotic system can be described as a random superposition of plane waves of the same wave number but different propagating direction.[36,37] Random plane wave (RPW) modeling gives predictions for both correlation functions above[36,38,39] which agree with the perturbation theory results for the diffusive regime[35,40]

$$\psi \Rightarrow e^{-|\mathbf{r}'|/l}J_0(k_F|\mathbf{r}'|), \tag{12}$$

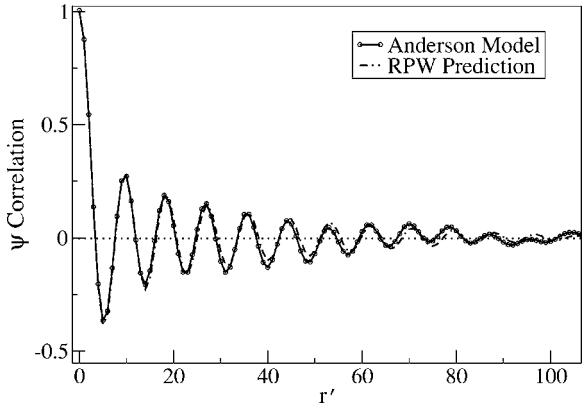

FIG. 4. Spatial correlation of the wave function in the diffusive regime. The data for $\langle\psi(\mathbf{r})\psi(\mathbf{r}+\mathbf{r}')\rangle$ is close to the random plane wave result, especially for small r'. Filling is 1/25, $W=0.5$, and $B=0$. To avoid boundary interference, we used a 30×30 section of the rectangle centered 1/4 of the side length from each boundary. Correlations were measured in the x direction from points within this section (y direction correlations are identical).

$$\psi^2 \Rightarrow 1 + 2e^{-2|\mathbf{r}'|/l}J_0^2(k_F|\mathbf{r}'|). \tag{13}$$

The ψ correlation should thus approach 0, and the ψ^2 correlation should approach 1 for large r'. Figures 4 and 5 display our results for the diffusive regime, and show good agreement with the RPW predictions, especially in the ψ correlation. At large distances, the correlations do appear to converge to the expected values, although we note visible discrepancies in the ψ^2 case.

The final characteristic we wish to consider before moving to statistics involving different eigenfunctions is the IPR distribution. Previously, we touched on the mean IPR values for different parameters, but Fig. 6 displays a histogram of IPR values for specific system realizations. As disorder increases across the three regimes, we see four important effects: the distribution gets wider and increasingly asymmetrical, and both the median and mode IPR values increase. In

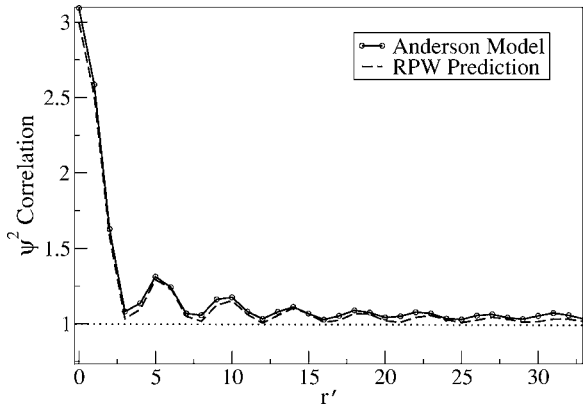

FIG. 5. Spatial correlation of the square of the wave function in the diffusive regime. Calculated results for $\langle\psi^2(r)\psi^2(r+r')\rangle$ are in reasonable agreement with the random plane wave result, especially for $r'<20$. RMT predicts that the correlation function should rapidly approach 1. See Fig. 4 caption for parameters.

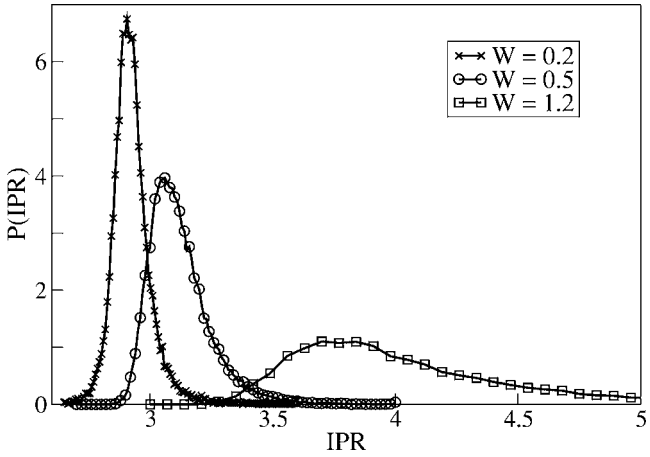

FIG. 6. Distribution of the inverse participation ratio (IPR) for the three different regimes (semi-ballistic at $W=0.2$, diffusive at $W=0.5$, and localized at $W=1.2$). At low disorder, the RMT/RPW prediction of a thin, Gaussian distribution is met. With increasing disorder, and even in the diffusive regime, the distributions become clearly asymmetric and increasingly wide. The integral under each curve is normalized to 1. (1/25 filling with $B=0$.)

the diffusive regime, the distribution is Gaussian-like near its maximum (as it should be given the smallness of the cumulants beyond the second one[27,41]), but the tails are clearly asymmetrical. In the large IPR tail, we find that the data follow an exponential distribution with a decay rate of $\simeq 8.0$ (obtained from fitting values larger than 3.4). Such an exponential decay is expected from calculations using the supersymmetric σ model.[21,27,42] For our parameters, the predicted decay rate is $\simeq 9.4$ [see, e.g., Eq. (3.92) in Ref. 21]. Considering that in our case $l \lesssim L$ while the σ model is valid for $l \ll L$, we find the good agreement between the σ-model result and our observation above to be another demonstration of the universality present in these systems. We will return in Sec. V below to make a detailed comparison with the analytic results for the magnitude and variance of the IPR in the context of the correlation between different wave functions.

We have now considered five separate statistics of varying complexity in the diffusive regime. Energy level spacing, probability distribution at a point, and the two spatial correlation statistics all are in excellent agreement with RMT and RPW predictions. We note, however, that the latter three statistics depend on individual sites alone and not system-wide, or global, characteristics. IPR, a global statistic, seems at this level to be within the general framework of expectations.

The establishment of this agreement serves two ends: justification that we are dealing with an authentic diffusive system of most relevance to mesoscopic physics, and confirmation that we are getting results for simple statistics that match previous work as well as analytical predictions. The latter demonstrates explicitly that the unexpected and complex correlations to be encountered in the next section are perfectly consistent with the simple and well-analyzed single-eigenfunction statistics familiar in disordered models, and so are likely to have wide application in disordered quantum physics.

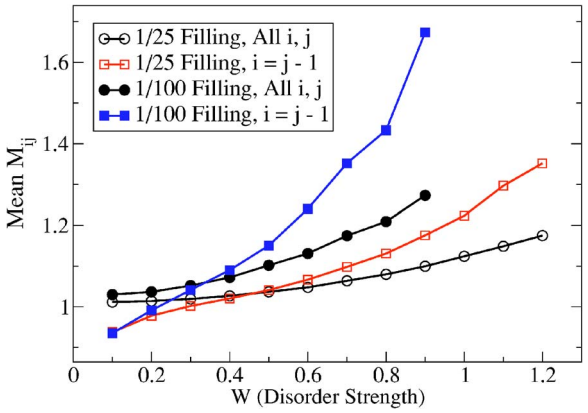

FIG. 7. (Color online) The mean of the M_{ij} as a function of disorder strength. When averaged over all wave functions in our energy window (circles), the mean rises roughly quadratically with increasing disorder strength from 1, the RMT value. In contrast, for consecutive energy levels ($i=j-1$, squares), the mean is suppressed below 1 at weak disorder and shows evidence of the three regimes. (Five disorder realizations with $B=0$.)

IV. CORRELATION OF DIFFERENT WAVE FUNCTIONS: DISAGREEMENT

The spatial similarity of different eigenfunctions is crucially linked to electron-electron interactions and so to the statistics of quantum dots in the Coulomb blockade regime. All data presented in this section are based on the quantity M_{ij}, defined as

$$M_{ij} = \mathcal{A} \int |\psi_i(r)|^2 |\psi_j(r)|^2 d^2r, \tag{14}$$

where i and j label different eigenfunctions. M_{ij} thus measures the system-wide, spatial correspondence between two eigenfunctions in a specific disorder realization. Note that M_{ii} is the IPR, discussed in the previous section.

RMT predicts no correlation between different eigenfunctions in the $N \to \infty$ limit. In this case of uncorrelated uniformity, and within the Weyl approximation

$$\langle |\psi_i(r)|^2 \rangle \simeq 1/\mathcal{A}, \tag{15}$$

mean M_{ij} should equal 1.0 for all $i \neq j$, the statistics of the M_{ij} should be independent of i or j, and there should be no correlation between different M_{ij}. This section demonstrates that these basic predictions of RMT and its simple extensions (such as RPW) are not met in our diffusive system.

A. $B=0$: Time-reversal invariant

We begin by studying M_{ij} in the simpler zero-field case. Figure 7 shows the trend in M_{ij} against disorder strength W, and also compares the average (on both i and j, in addition to disorder) for all $i \neq j$ in the band with the average (on j and disorder) for consecutive eigenfunctions. In all cases, the mean M_{ij} appears to converge to 1 for very low W values, but are consistently higher elsewhere. As in Fig. 1 which shows IPR as a function of W, M_{ij} rises with increasing disorder, and does so rapidly for consecutive eigenfunctions

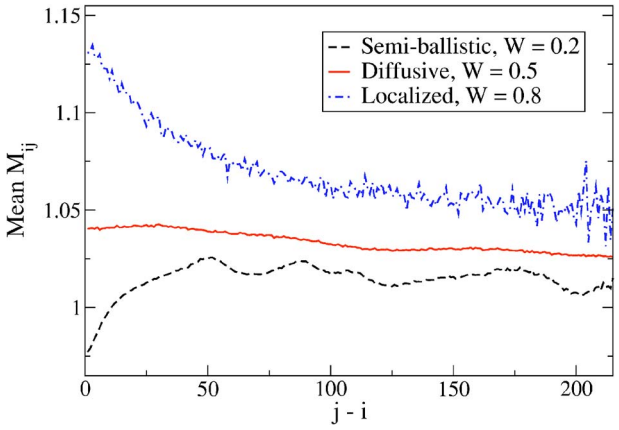

FIG. 8. (Color online) The dependence of mean M_{ij} on the spacing between the two states for the three different regimes (semiballistic at $W=0.2$, diffusive at $W=0.5$, and localized at $W=0.8$). The point at which $j-i=0$, corresponding to the IPR, is omitted for clarity. The mean increases with W, and the effect is magnified for close eigenfunctions. Note that the curve for the diffusive system is nearly flat. (1/25 filling with $B=0$.)

at 1/100 filling. Again mirroring the IPR dependence, M_{ij} is higher at the lower energy and rises sluggishly at 1/25 filling. Note that for both energy levels the points at which the plots for consecutive and total M_{ij} cross are near the chosen values for diffusivity: $W=0.35$ for 1/100 filling and $W=0.5$ for 1/25 filling. Finally, we note that calculations for a torus (periodic boundaries in each direction) yielded a mean M_{ij} significantly closer to 1.0 for most parameters.

One remarkable feature of Fig. 7 is that the mean (over disorder and j) of M_{ij} for consecutive eigenvalues $i=j-1$ is substantially different from the result obtained by further averaging this quantity over the index i, implying some degree of disorder and energy dependent correlations between the eigenfunction. To investigate this further, Fig. 8 plots mean M_{ij} against $j-i$, indicating the correlation's dependence on the nearness in energy of the two eigenfunctions. We guess from Fig. 8 that the points of intersection in Fig. 7 represent the disorder levels at which M_{ij} is approximately constant against the difference in i and j, which we thus presume to be a characteristic of diffusive systems. In comparison, the semiballistic system displays a slightly negative correlation for close energies and positive correlation for for distant energies. The localized system has a stronger positive correlation for close energies—states which are nearby in energy tend to overlap in space—which decreases as the energy difference increases. Note that this is exactly the opposite of the well-known trend in the strongly localized case: when $L_{\mathrm{loc}} \ll L$, states that are close in energy tend to occupy different parts of the sample.[18,19] It is quite surprising that modest changes in W could so drastically change how energy correlation operates in a system, going from increasing with energy difference to staying constant to decreasing and presumably back to increasing in the strong localization limit.

We cannot, at this time, claim that we understand the origin of the energy correlation between the wave functions leading to the behavior observed for the M_{ij}'s in Fig. 8. In analytic treatments, the energy scale known as the Thouless energy plays an important role: for diffusive systems, $E_{\mathrm{Th}}=\hbar D/\mathcal{A}$ is the energy scale related to the time $t_D=\mathcal{A}/D$ needed to diffuse across the whole system. In both the supersymmetric σ model and RMT/RPW approaches, the expectation is that the mean M_{ij} would be independent of i-j for energy differences less than E_{Th} and then approach 1 rapidly as a power law, $\propto 1/(i-j)^2$ [see, e.g., Eq. (3.84) in Ref. 21]. This is clearly not the case in our data. We would like, however, to mention that, from a qualitative point of view, the observed energy correlation would be compatible with the existence of a relatively small number of *localized resonances*.

What we mean by a localized resonance is, in a very schematic way, what would result from the following picture. Assume one can define an approximation H_0 of the Anderson Hamiltonian (1) such that the eigenstates of H_0 can be divided in two classes: a vast majority of delocalized states ψ_i^0, and a smaller number of very localized states φ_l such that $\mathrm{IPR}_{\varphi_l} \gg 1$. In fact, states which are in some sense "anomalously localized" are known to exist from supersymmetric σ-model investigations.[20,21] Let us furthermore assume that the perturbation $V=H-H_0$ couples the φ_l to the ψ_i^0 with matrix elements whose typical magnitude v is large compared to the mean level spacing Δ, but small enough in terms of the energy spacing of the φ_l that these latter remain essentially decoupled.

In such a circumstance, we can model the eigenstates ψ_i of the full Hamiltonian H near the energy ϵ_l of φ_l using a resonant level model, implying that

$$\psi_i = a_i \psi_i^{\mathrm{deloc}} + f_\Gamma(\epsilon_i - \epsilon_l)\,\eta_i \varphi_l. \tag{16}$$

Here, ψ_i^{deloc} is a delocalized wave function orthogonal to φ_l (and not necessarily close to ψ_i^0), η_i is a fluctuating quantity of r.m.s. 1, and the smooth positive function $f_\Gamma(\epsilon-\epsilon_l)$ of width $\Gamma \sim v$ describes the envelope of the resonance. The resonance contains approximatively $N_{\mathrm{res}}=\Gamma/\Delta$ levels, and normalization imposes that within the resonance (i.e., for $\epsilon_i - \epsilon_l \leqslant \Gamma$), $f_\Gamma^2 \simeq 1/N_{\mathrm{res}}$. If N_{res} is large enough, the normalization factor a_i is not very far from 1, and we shall drop it from now on.

If Eq. (16) is a good model for the eigenstates of H near the resonance, we see that, in this region of energy, the envelop of the M_{ij} should be given by (neglecting terms of order $1/N_{\mathrm{res}}$)

$$\langle M_{ij} \rangle \simeq 1 + f_\Gamma^2(\epsilon_i - \epsilon_l) f_\Gamma^2(\epsilon_j - \epsilon_l)\mathrm{IPR}_{\varphi_l}. \tag{17}$$

If IPR_{φ_l} is not negligible compared to N_{res}^2, such an expression provides a mechanism for increasing the mean value of M_{ij}, and furthermore would explain that this enhancement is larger if i and j are close in energy since this increases the probability that they belong to the same resonance.

In the case of a torus (periodic boundary conditions), we found that the enhancement of the M_{ij}'s is smaller. We interpret this as implying that the localized resonances are preferentially created near the hard wall boundaries of the system; this is actually the region where we see the first localized states appear as disorder is further increased.

To finish this subsection, we comment briefly on two points. First, we mention that one statistic that may help explain some features of M_{ij} is the correlation of the wave function with the disorder configuration of the system, defined as

$$C_j = \sum_r \left(\psi_j^2(r) - \frac{1}{\mathcal{A}} \right) \epsilon(r), \tag{18}$$

where $\epsilon(r)$ is the on-site disorder at r and $\mathcal{A}$ is the area of the system. Our computational results demonstrate that this disorder correlation, negative (for filling smaller than one half) for all W values, is proportional to the square of the disorder strength and, in fact, matches the value derived from perturbation theory. Since individual wave functions in a specific system are correlated to the same disorder configuration, they will be correlated to one another. It should be stressed, however, that the amount of correlation thus induced is much smaller than that seen in the M_{ij} data.

We finally note in passing that several statistics show periodic structure as a function of energy. The mean IPR and disorder correlation, for example, show small oscillatory effects when plotted against eigenfunction number. As the trends are more prominent in the torus or smaller systems, they are most likely due to periodic orbit effects. However, persistence of this odd behavior when the smallest period is about four times the mean free path, suggests some extra relationship may influence how wave functions at specific energies interact.

B. $B \neq 0$: Broken time-reversal symmetry

Because we want to eventually study interaction effects in the Coulomb blockade regime, and for these latter the discussion of the zero magnetic field case is made more complicated by the partial screening of the Cooper channel,[2,43] we shall now consider a situation where a magnetic field is applied, effectively suppressing the time reversal invariance of the system. For the Coulomb blockade, we should like to choose a system in the diffusive regime containing a few hundred electron. These considerations lead us to pick the following parameters: 1/100 filling corresponding to about level 400; $W=0.35$; and $B=6$, the field strength at which the statistics indicating broken time-invariance appear to level off as a function of B. We also wish to supplement this system with data for an intermediate energy range. Thus, three such systems will be investigated: Our favored system at 1/100 filling and $W=0.35$; a system at 1/25 filling and $W=0.5$, for comparison with the $B=0$ case; and an intermediate system at 1/75 filling and $W=0.5$.

Our first concern is to establish that the three systems with nonzero magnetic field are diffusive. Figure 9 plots each system's energy level spacing distribution along with the relevant Wigner surmise (GUE for broken time-reversal invariance). We see excellent agreement in all three cases, an indication of diffusivity. In addition, note that the discussion of length scales—mean free path, system size, and localization length—in Sec. III holds unchanged for the weak field considered, and so suggests diffusivity in each of our three cases. Furthermore, simple statistics like IPR and probability

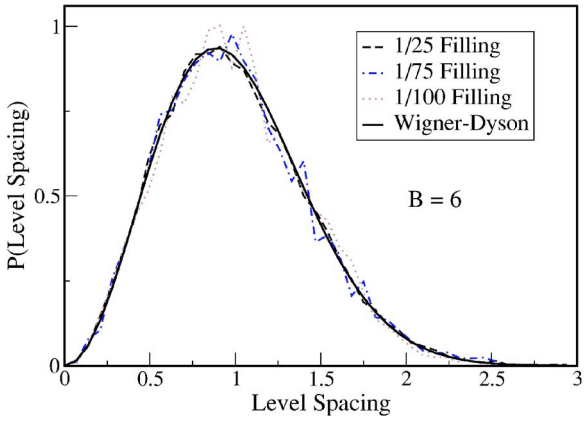

FIG. 9. (Color online) Energy level spacing distribution in a magnetic field large enough to break time-reversal symmetry (6 φ_0 through $2\pi\mathcal{A}$). The curves at three different energies, all in the diffusive regime, match the corresponding Wigner surmise of RMT (solid). Both the mean and integral are normalized to 1.

distribution (not shown) match RMT-based predictions reasonably well. A final confirmation is assurance that the cyclotron radius

$$R_c = \frac{m v_F}{eB'} = \frac{k_F \mathcal{A}}{2\pi} \tag{19}$$

is much larger than the system. Indeed, finding k_F from the dispersion relation yields at $B=6$

$$R_c(1/25 \text{ filling}) = 830,$$

$$R_c(1/75 \text{ filling}) = 490,$$

$$R_c(1/100 \text{ filling}) = 400, \tag{20}$$

all considerably larger than the system size (264) or the mean free path. We can thus be reasonably assured of diffusivity in these three systems.

Figure 10 displays M_{ij} data against closeness of energy for our favored 1/100 filling system: the mean and median are compared as well as the standard deviation. All three plots have a characteristic shape: a rapid rise as i-j decreases from about 50 to 3 followed by a tiny dip from about 3 to 1. As the pattern is closest in form to the slightly localized $B=0$ case, it is possible that the application of a magnetic field may be strengthening prelocalization effects. However, this basic form holds at nonzero magnetic field even for weak disorder (not shown), discrediting the notion that we are seeing genuine localization at these parameters. Note that the mean M_{ij} is consistently higher than the median, and significantly larger for close energies. Indeed, the distribution of M_{ij} is strongly asymmetrical for close i, j, and increasingly Gaussian for more distant eigenfunctions. As for the $B=0$ case, the observed energy dependence in the mean and distribution of M_{ij} are neither seen in nor expected from analytic results to date.

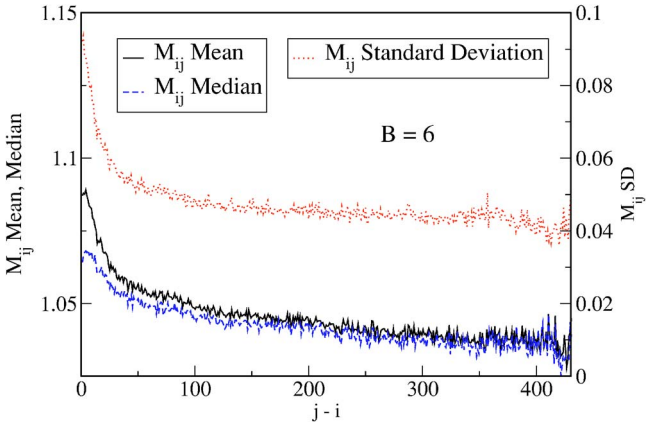

FIG. 10. (Color online) Mean, median, and standard deviation of M_{ij} as a function of the spacing between the two states. The scale for the standard deviation is on the right, and the point $j=i$ is omitted for clarity. The similarity in form of the mean and the standard deviation, as well as the increasing disparity between mean and median with closeness in energy, are striking. (1/100 filling, $W=0.35$, $B=6$.)

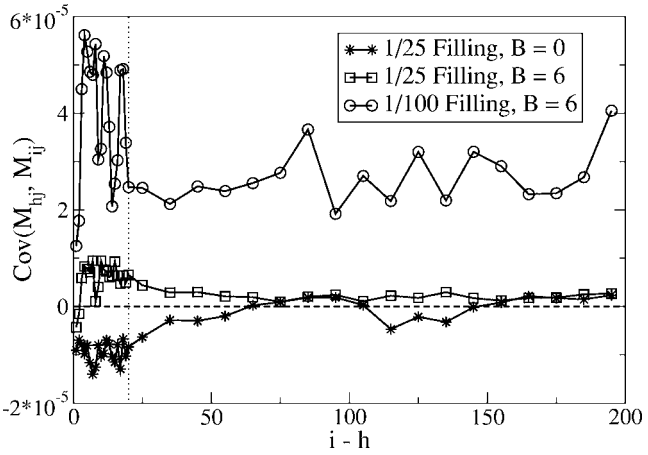

FIG. 11. Covariance of M_{hj} and M_{ij} (distinct h, i, j) in three diffusive cases as a function of the spacing between i and h, averaged over all j in the energy window. For clarity, the first ten points in each plot are shown intact, whereas the remaining points are averaged in groups of 10. Note the qualitative difference at 1/25 filling between the zero field and $B=6$ cases.

C. Interaction terms

The M_{ij} enter directly into interaction terms for the Coulomb blockade peak spacing through F_j, defined as

$$F_j[n] = \sum_{i=j-n}^{j-1} M_{ij} - \overline{M_{ij}}, \tag{21}$$

where the $\overline{M_{ij}}$ average (over disorder) subtracted from each M_{ij} is calculated from the same system parameters and eigenfunctions. Note that $\overline{M_{ij}}$ depends on the eigenstate indices i and j. The disorder average of F_j is thus 0, by definition. The specific term included in the peak spacing calculation is $(F_{j+1}[n]-F_j[n])$, whereby a larger magnitude will lead to wider peak spacing and spin distributions. We are thus interested in the root-mean-square of $(F_{j+1}[n]-F_j[n])$, given by $(\overline{F_{j+1}^2}[n]+\overline{F_j^2}[n]-2\overline{F_{j+1}[n]F_j[n]})^{1/2}$. As we show below, this quantity is dominated by the $F_j^2[n]$ terms, particularly in the higher-energy systems.

A quick calculation shows that the $\overline{F_j^2}[n]$ component is a sum of n variance terms and $(n^2-n)/2$ covariance terms:

$$\overline{F_j^2[n]} = \sum_{i=j-n}^{j-1} \mathrm{var}(M_{ij}) + 2\sum_{h=j-n}^{j-2}\sum_{i=h+1}^{j-1} \mathrm{cov}(M_{hj},M_{ij}). \tag{22}$$

We plot the square root of $\mathrm{var}(M_{ij})$ against j-i for 1/100 filling in Fig. 10. Note once again the striking energy dependence. As a precursor to the $F_j^2[n]$ data, the covariance statistics are presented in Fig. 11 as a function of i-h. Note the qualitative difference between the $B=0$ and $B=6$ cases in that the covariance is negative without an applied magnetic field and positive with one. We have as yet no explanation for this difference. Another important feature is that the finite magnetic field covariance is constant (though small) for nearly all i-h. Finally, the covariance is noticeably larger for the lower-energy case. Aspects of the behavior of the covariance of the M_{ij} beyond RMT can, no doubt, be captured with the supersymmetric σ-model approach;[21,44] however, we are not aware of any results along these lines at this time.

Figure 12 depicts the resulting root-mean-square of $F_j[n]$ as a function of n, averaged for all j in the energy band. All four systems considered in this paper are shown, and the quantitative and qualitative differences between them are clear. $F_j[n]$ becomes much larger for low filling cases, mainly due to the larger variance of M_{ij}. At $n=400$, $F_j[n]$ in the $B\neq 0$, 1/25 filling case is rising more rapidly with n than the zero field case because of the positive covariance in the former.

All four cases are noticeably different from the usual expectation for the behavior of $F_j[n]$. The expectation from RMT and random plane wave considerations is that M_{ij} for different states nearby in energy are uncorrelated and have the same variance. Thus, $\mathrm{var}(F_j[n])$ increases linearly at small n as uncorrelated variables are added. However, the RMT modeling is only expected to apply up to $\delta E_{ij}=E_i-E_j$ of order the Thouless energy $E_{\mathrm{Th}}=\hbar D/\mathcal{A}$. Beyond E_{Th}, one can distinguish in principle two energy ranges[45] separated by the elastic scattering time τ: (i) a first energy range $E_{\mathrm{Th}} < \delta E_{ij} < \hbar/\tau$ corresponding to diffusive motion unaffected by the boundaries and (ii) $\hbar/\tau < \delta E_{ij}$ which is associated with the ballistic part of the dynamics.

It is usually thought that the second of these energy ranges will be associated with the *saturation* of mesoscopic fluctuations. To understand the origin of this thinking, consider a quantity similar to $F_j[n]$ but significantly simpler to analyze

$$N_j[n](\mathbf{r}) = \sum_{i=j-n}^{j-1} [|\phi_i(\mathbf{r})|^2 - 1/\mathcal{A}]. \tag{23}$$

The magnitude of the fluctuations of $N_j[n](\mathbf{r})$ can be shown to be related to the probability of return of a trajectory to its original point $\mathbf{r}$. However, the elastic time τ sets a minimum

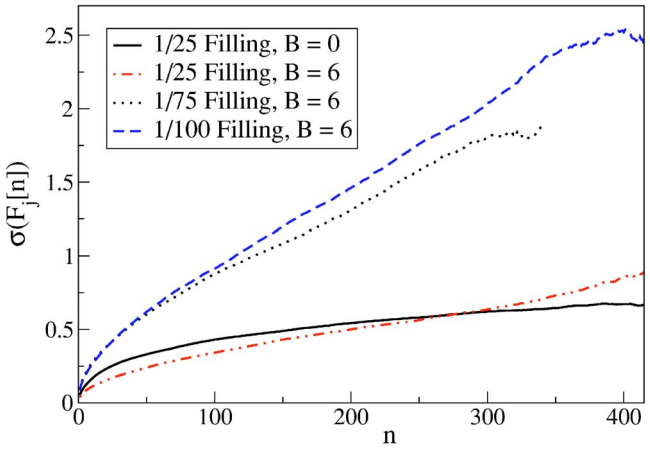

FIG. 12. (Color online) Standard deviation of $F_j[n]$ for all four diffusive systems, averaged over all j in the energy window. The magnitude is surprisingly large. Predictions that $F_j[n]$ would quickly saturate are not met; this is seen most clearly in the presence of a magnetic field where the increase is roughly linear even at $n=400$.

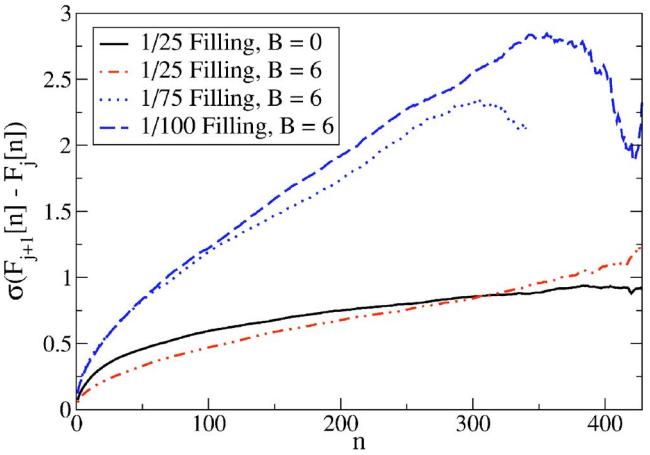

FIG. 13. (Color online) The root-mean-square of $(F_{j+1}[n] - F_j[n])$ for all four diffusive systems, averaged over all j in the energy window. This quantity is directly relevant to Coulomb blockade peak spacing. Although similar to those in Fig. 12, the curves are not simply $\sqrt{2}$ r.m.s. $(F_j[n])$ because of correlations between $F_{j+1}[n]$ and $F_j[n]$ that are largest at low energy. As in Fig. 12, the magnitude is surprisingly large.

time before which no trajectory can return. As a consequence, no fluctuations are added by the energy range $\hbar/\tau < \delta E_{ij}$.

In the same way, it seems natural to expect that any mesoscopic fluctuation would saturate for energy larger than $\hbar/\tau$. The systems we are investigating furthermore have been chosen in such a way that the elastic mean free path l is not much smaller than the size L_x of the rectangle. As a consequence, the Thouless energy is not very different from the scale $\hbar/\tau$.

Thus, what we expect to see is a linear rise of the variance of $F_j[n]$, followed by a saturation when δE_{ij} reaches an energy not much larger than the Thouless energy. This would also be the expected behavior for a ballistic system, provided one defines the Thouless energy as $E_{\mathrm{Th}}=\hbar/t_f$, where t_f is the time of flight across system. For the parameters used here, the value of n at which we expect to see saturation n_{Th} is 20–45 for 1/25 filling and 10–25 for 1/100 filling.

What we observe, however, is a continued rise *for all n*, particularly with the inclusion of a magnetic field. In the case of 1/100 filling, we are near the bottom of the band, and the sum in $F_j[n]$ provides a good estimate for summing over all the filled levels. Note that the continued linear increase of the standard deviation in the $B\neq 0$ cases requires correlation among the M_{ij}.

The only component not yet considered is the mean of $F_{j+1}[n]\cdot F_j[n]$, which one might expect to be about as large as $F_j^2[n]$, thereby making var $(F_{j+1}[n]-F_j[n])$ small. Although the statistic does similarly rise with n, it turns out to be considerably smaller than $F_j^2[n]$: in both the 1/25 and 1/100 cases with magnetic field, this component reaches about one-fifth of the value of $F_j^2[n]$ for the largest n.

Finally, Fig. 13 depicts the quantity directly relevant for the Coulomb blockade peak spacing calculation, the root mean square of $(F_{j+1}[n]-F_j[n])$, averaged for all j in the spectrum. Showing remarkable similarity to the plot for $\sigma(F_j[n])$ alone, including the order of magnitude, Fig. 13 contains odd features at the end of the 1/75 and 1/100 filling plots that could either be noise caused by fewer eigenfunctions being considered or real system effects involving the very lowest eigenfunctions in the system. The most important feature of Fig. 13, however, is the sheer size of the Coulomb blockade-relevant statistic, even at high energies. When added to the peak spacing calculation, a statistic on the order of 1 cannot help but cause major changes to system behavior.

The end result of this section has been to demonstrate complex, unexpected behavior in the energy correlations of diffusive wave functions, behavior that we will demonstrate has a major effect on the statistics of the Coulomb blockade.

V. COMPARISON TO ANALYTIC RESULTS

We pause briefly from our main development to compare our results for the M_{ij} to existing analytic results, particularly those from supersymmetric σ model[21,27,42] and random plane wave[41] calculations. The quantities we focus on are the mean and standard deviation of the IPR and off-diagonal M_{ij}. These are given in the first six lines of Table I for our standard four cases. Our interest, in particular, is in the deviation of these values from the universal values obtained in the simplest RMT—namely, that the mean should be integer (1, 2, or 3 depending on the case) and the standard deviation should be 0. We also give in the table the values for $F_j[415]$ and the covariance, the quantities showing the most unexpected results. No comparison of these will be made to analytic results, however, because no such results exist.

There are two caveats that one should bear in mind in making a comparison between the analytic results and our data. First, the analytic results are primarily for eigenfunctions that are close by in energy, within E_{Th} of each other. There are no previous results, as far as we know, for our

TABLE I. The energy correlation statistics most relevant to real mesoscopic systems are displayed for the four systems considered in this paper. In comparing system behavior, recall that the 1/100 filling system is at a lower W value (0.35 compared to 0.5) than the other systems, which was done to ensure it was diffusive. To see the effect of lowering energy while keeping the disorder value constant, one can compare 1/25 and 1/75 filling. Note also the marked differences between the zero and nonzero magnetic field cases at constant energy.

Statistic	1/25 filling, $B=0$	1/25 filling, $B=6$	1/75 filling, $B=6$	1/100 filling, $B=6$
Mean IPR	3.12	2.14	2.36	2.29
Mean $M_{i-1,i}$	1.04	1.05	1.11	1.09
Mean M_{ij}	1.03	1.03	1.06	1.05
σ(IPR)	0.129	0.082	0.197	0.203
$\sigma(M_{i-1,i})$	0.053	0.039	0.097	0.092
$\sigma(M_{ij})$	0.044	0.026	0.056	0.053
r.m.s.(F_j[415])	0.67	0.89	N/A	2.42
r.m.s.(F_{j+1}[415]$-F_j$[415])	0.93	1.10	N/A	2.07
Mean cov(M_{hj},M_{ij})	-2.8×10^{-6}	3.1×10^{-6}	2.9×10^{-5}	2.8×10^{-5}
Mean corr(M_{hj},M_{ij})	−0.0016	0.0055	0.0097	0.0106

main finding that $F_j(n)$ grows for large n because of correlations between eigenstates widely separated in energy. The second caveat is that the σ-model results are obtained in a somewhat different regime from our numerics: the σ-model assumes $l \ll L$ while for our numerical results $l \lesssim L$.

The analytic approaches predict that three trends should be present in the data. First, the energy dependence: the deviations from simplest RMT should be proportional to the square root of the filling.[21,41] For our data, then, the deviations in the 1/100 filling column should be twice those at 1/25 filling (both at $B=6$). We see that for the mean, this is certainly the case. For the standard deviation, the ratio ranges from 2.5 for the IPR to 2.0 for the far-off-diagonal case. Thus, this trend is quite reasonably obeyed by our data.

Second, in the analytic approaches, the statistics of the IPR, M_{ii}, is simply related to the statistics of the off-diagonal terms M_{ij}. For the mean of the distribution, the σ-model approach yields[21]

$$\frac{\langle \mathrm{IPR}\rangle_{B=0}-3}{\langle M_{i\neq j}\rangle_{B=0}-1}=3, \quad \frac{\langle \mathrm{IPR}\rangle_{B\neq 0}-2}{\langle M_{i\neq j}\rangle_{B\neq 0}-1}=2. \tag{24}$$

Our $B=0$ data is in good agreement with this result, for both the nearest neighbor values $(i,i-1)$ and the far-off-diagonal terms M_{ij}. Note, however, that the ratio for our $B=6$ data differs sharply from the above: for nearest neighbors the ratio is about 3 and increases to 5 or 6 for the far-off-diagonal terms. Turning to the standard deviation of the distribution, there are no σ-model results, but the RPW approach yields[41]

$$\frac{\mathrm{r.m.s.(IPR)}_{B=0}}{\mathrm{r.m.s.}(M_{i\neq j})_{B=0}}=\sqrt{6}, \quad \frac{\mathrm{r.m.s.(IPR)}_{B\neq 0}}{\mathrm{r.m.s.}(M_{i\neq j})_{B\neq 0}}=2. \tag{25}$$

Good agreement is obtained for both of these ratios in the case of nearest-neighbor terms $M_{i,i-1}$, but the far-off-diagonal terms show smaller fluctuations and so are not in agreement. Overall, then, the agreement between our data and this analytic trend is mixed: the results for the mean at zero field and the fluctuation of the nearest-neighbor terms is good, but those for the mean at nonzero field and the fluctuation of far-off-diagonal terms is poor.

The third predicted trend is, of course, the relation between the results at zero magnetic field and those at nonzero field. For the mean, the σ model yields[21]

$$\frac{\langle \mathrm{IPR}\rangle_{B=0}-3}{\langle \mathrm{IPR}\rangle_{B\neq 0}-2}=3, \quad \frac{\langle M_{i\neq j}\rangle_{B=0}-1}{\langle M_{i\neq j}\rangle_{B\neq 0}-1}=2. \tag{26}$$

In our data, however, the deviations in the mean are approximately independent of magnetic field. For the fluctuations, those of the IPR are expected to be larger by a factor of 3 in the presence of time-reversal symmetry.[21] We see a factor of 1.6 in our data. Thus there is a striking disagreement between the σ-model treatment and our numerics in terms of the effect of a weak magnetic field.

To summarize our results with regard to the trends, some of the analytic predictions are seen in our data but others are not: the energy dependence checks, the behavior of the IPR compared to off-diagonal terms is mixed, and, most strikingly, the expected effects of breaking time-reversal symmetry are just not seen in the data. With regard to the latter, we emphasize that the simpler effects of breaking time-reversal symmetry, such as the change in level spacing distribution or distribution of $|\psi(r)|^2$, are certainly seen in our data, so the discrepancy here is not simply a matter of having applied too weak a field.

To make a more exacting comparison of the data and analytic results, we now compare the absolute magnitude of the deviation of the mean and the variance of the distribution. In order to do this, we need to first settle on a value for g, the dimensionless conductance, which is the main parameter controlling the expansion in the σ-model results. Standard expressions exist for the conductance g_{diff} in the strongly diffusive limit ($l \ll L$) as well as for g_c, the ballistic conductance ($l \gg L$) assuming random scattering on the boundaries. For our parameters we find at 1/25 filling $g_{\mathrm{diff}}=36$ and $g_{\mathrm{ball}}=16$ while at 1/100 filling the values are $g_{\mathrm{diff}}=16$ and $g_{\mathrm{ball}}=7.9$. Our system is intermediate between these two limits. Surely the conductance cannot be larger than g_{ball} as this is the fundamental bound coming from the finiteness of the system. In fact, as a function of system size L while

keeping other parameters constant, the conductance should cross over from $g_{\rm ball} \propto L$ to the value $g_{\rm diff}$ which is independent of L. As our system is clearly in this crossover region, use of an interpolation formula appears necessary. We use the simplest such formula: $g_{\rm eff}^{-1} = g_{\rm diff}^{-1} + g_{\rm ball}^{-1}$. Thus the conductance values we use are $g_{\rm eff} = 11$ for 1/25 filling and $g_{\rm eff} = 5.3$ for 1/100 filling.

With these values for $g_{\rm eff}$, the σ-model expressions[21] in the diffusive limit are easily evaluated. As the trends have been discussed above in detail, we give only a few representative values here. In the absence of time-reversal symmetry, we find

$$\langle \mathrm{IPR} \rangle - 2 = 0.044, \quad \text{r.m.s.(IPR)} = 0.084 \tag{27}$$

at 1/25 filling and

$$\langle \mathrm{IPR} \rangle - 2 = 0.096, \quad \text{r.m.s.(IPR)} = 0.18 \tag{28}$$

at 1/100 filling. Comparing with the table, we see that for the fluctuations the numerical data are in good agreement with the diffusive σ-model results. In contrast, the deviation of the mean IPR from the RMT value is rather far off from the σ-model predictions above. It is curious that once the scaling is done to change these values to those appropriate in the presence of time-reversal symmetry [Eq. (26)], the fluctuations are not in agreement while the mean value of the IPR is.

To summarize this section, we saw that there is already for the M_{ij} statistics some substantial differences between our computational result and extensions of random matrix theory via the σ model. Some of these differences are merely quantitative, and might be explained by the fact that the regime we consider, where the mean free path is of order the system size, is not the one typically considered in σ-model calculations. Other differences, such as the existence of correlations among the M_{ij} are qualitative, and thus less expected.

The second kind of "integrated" statistics that we have considered concerns the F_j's, which involve a further summation over states. For these quantities, we are not aware of any analytic results. The fluctuations of the F_j's show, however (see Fig. 13) an absence of saturation which is in total contradiction with intuition developed for simpler quantities.

All these differences suggest that disordered quantum systems may be a tougher nut to crack than previously thought.

VI. APPLICATION TO THE COULOMB BLOCKADE

A major way to probe the energy properties of electrons in a disordered media is by constraining groups of electrons in a quantum dot and studying the electrical transport of individual electrons across the dot. The electrostatic charging energy being large, the dot is usually constrained to remain with a fixed number of electrons, which prevents current to flow at small bias voltage. This Coulomb blockade effect is essentially classical, and allows an applied gate voltage V_g to be adjusted so that the energy for N electrons is the same as that for $N+1$, thereby inducing a finite conductance. The conductance through the dot as a function of V_g therefore forms a series of sharp peaks, the height and position of which encode information about the dot's ground state.[46]

The peak spacing, with which we are most concerned here, is proportional to the second difference of the ground-state energy with respect to electron number N:

$$\Delta^2 E_N \equiv E_{\rm g.s.}(N+1) + E_{\rm g.s.}(N-1) - 2E_{\rm g.s.}(N), \tag{29}$$

which varies because of changing interaction effects as electrons are added and produces a peak spacing distribution. The simplest model of this distribution results from writing the ground state energy as the sum of the classical charging energy and the energies of the occupied single particle states, known as the constant-interaction (CI) model. The ground state energy in this model can therefore be written in terms of the occupation numbers $n_{i\sigma}$ and one particle energies ϵ_i as

$$E_N^{\rm CI} = (Ne)^2/2C + \sum_{i\sigma} n_{i\sigma}\epsilon_i, \tag{30}$$

where $n_{i\sigma} = 1$ for the N lowest orbitals and zero otherwise.

As a consequence, one gets the simple prediction

$$\Delta^2 E_N = e^2/C \text{ for odd } N,$$

$$\Delta^2 E_N = e^2/C + (\epsilon_{N/2+1} - \epsilon_{N/2}) \text{ for even } N. \tag{31}$$

The drastic odd/even difference is a quantum effect resulting from the spin of the electron.

Although to our knowledge no quantum dot experiment has been conducted in the low temperature diffusive regime relevant to our study, all but one of the experimental results produced so far for quantum dots show a marked disagreement with the prediction in Eq. (31)(for a recent discussion see Ref. 47; the exception[48] is the case of a quantum dot formed from a carbon nanotube). They show a wider peak spacing distribution and the lack of a pronounced odd/even effect. This has made it clear that the effect of the residual screened interaction between electrons is important in the description of Coulomb blockade experiments. A simplified but reasonably good approximation for this residual interaction is a zero-range repulsive potential

$$V_{\rm sc} = \frac{2J_s}{\nu_0^{(2)}} \delta(\mathbf{r} - \mathbf{r}') \tag{32}$$

with $\nu_0^{(2)}$ the total density of states (including spins) and J_s a parameter that can be taken as the Fermi liquid parameter $f_0^{(a)}$. We consider a case with moderate interactions: the value of r_s, the usual parameter to characterize the strength of interactions in an electron gas, is 1.5. For this value, Monte Carlo calculations[49] give $f_0^{(a)} \simeq 0.4$, and we shall use this value of J_s in what follows.

It is known that in the absence of magnetic field, perturbative calculations in this residual interaction should include higher order terms (the so called Cooper channel) which makes the discussion significantly more involved.[2,43] We shall therefore restrict ourselves to the discussion of nonzero magnetic field, for which a first order perturbation calculation is appropriate. In that case, the eigenstates are still Slater determinants characterized by occupation numbers $n_{i\sigma} = 0, 1$. Noting that for a zero-range interaction such as Eq. (32) the exchange term exactly compensates the direct one for same

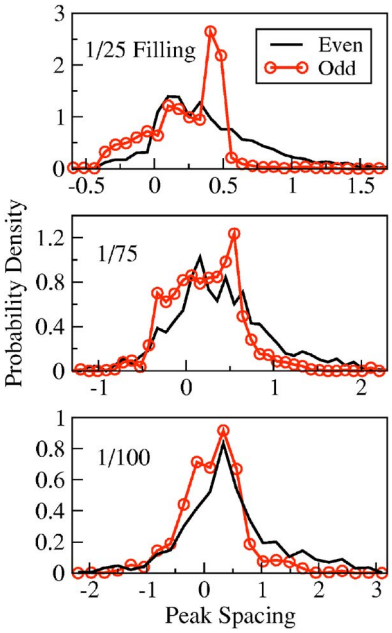

FIG. 14. (Color online) Peak spacing distributions for the three systems with $B=6$ flux quanta and $J_s=0.4$. The integral under both the odd and even curve is normalized to 1, and both curves are shifted left a distance J_s, as is customary. Note the wide spacing distribution, the depression of the odd peak at J_s, and the lack of a strong odd/even effect, all increasingly apparent as energy is lowered.

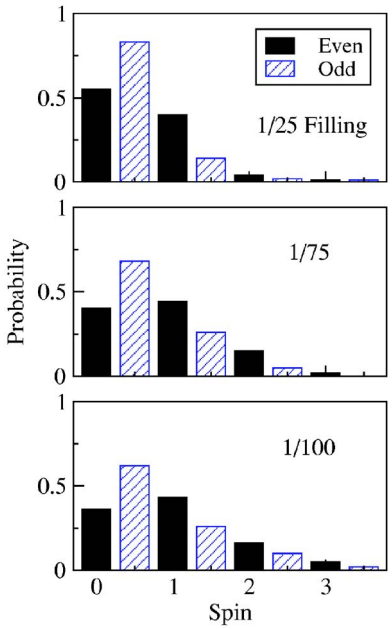

FIG. 15. (Color online) Spin distributions for the three systems with $B=6$ flux quanta and $J_s=0.4$. Note that the average net spin increases as energy is lowered, and even at 1/75 filling, a spin of 1 is more likely than a spin of 0. The demonstrated spins are much larger than are predicted in most theories.

spin electrons, their energy is given by $E[n_{i,\sigma}]=E_{\mathrm{CI}}[n_{i,\sigma}]+E_{\mathrm{RI}}[n_{i,\sigma}]$ where $E_{\mathrm{CI}}[n_{i,\sigma}]$ is the constant interaction contribution Eq. (30) and

$$E_{\mathrm{RI}}[n_{i,\sigma}]=\Delta\frac{J_s}{2}\sum_{i,j,\sigma\neq\sigma'} n_{i,\sigma}n_{j,\sigma'}M_{ij} \tag{33}$$

is the residual interaction correction. For a given set of one particle energies ϵ_i and wave functions ψ_i (thus fixing the M_{ij}), the ground state is then obtained by minimizing $E[n_{i,\sigma}]$ under the constraint that $\Sigma n_{i,\sigma\sigma}=N$. Because of the residual interaction term, this might not correspond to filling the N lowest one particle orbitals, and in particular may imply nontrivial (i.e., not zero or one-half) spin $S=\Sigma_i n_{i,+}-\Sigma_i n_{i,-}$ (with $+$ and $-$ the minority and majority spins, respectively).

If one assumes, however, the ground state occupation numbers are the same as in the absence of interaction, Eq. (31) is just modified to

$$\Delta^2 E_N = e^2/C + M_{N+1,N+1} \text{ for odd } N,$$

$$\Delta^2 E_N = e^2/C + (\epsilon_{N/2+1}-\epsilon_{N/2}) + F_{j+1}[n]-F_j[n] \text{ for even } N. \tag{34}$$

Thus, the surprisingly large variance in both the M_{ij}'s and F_j's may contribute greatly to the wider-than-expected peak spacing distribution observed[47] experimentally.

To confirm this, we applied the same eigenfunctions gleaned for the previous sections directly to a Coulomb blockade calculation. All of the applied eigenfunctions have broken time-reversal symmetry and the interaction strength used is $J_s=0.4$. We show both the peak spacing distribution (Fig. 14) and net spin of the system (Fig. 15) for all three of our relevant models.

The CI+RMT model, in comparison to Fig. 14, shows a total concentration at zero for odd N and an asymmetric Wigner-Dyson-type distribution from about 0 to 1 for even N. Other models, such as those relying on density functional theory, show departures from that basic structure, but typically show a peak at J_s for odd N and a comparatively thin distribution for even N. Our results predict that diffusive systems should display a much wider peak spacing distribution and a disappearance of the odd/even effect. Both effects are increasingly marked at lower energies, which is also closer to the ideal inclusion of all energy states from the ground level up.

The total spin is also much larger than most models predict, which is similarly likely due to interaction effects between distinct eigenfunctions. Thus, one prediction from this study is the presence of a *large total spin in electrons constrained in a diffusive quantum dot* at low temperature.

VII. CONCLUSION

We have demonstrated that certain properties of disordered quantum dots are very different from expectations based on random matrix theory or random plane wave considerations. The key element in the properties which show these discrepancies is that they involve wavefunctions at different energies and an integral over space. They are properties which are both *"off-diagonal" in energy and global in space*.

For these quantities, the mesoscopic fluctuations that we see are much larger than expected. Apparently the correlation among the wavefunctions amplifies the fluctuation effects. We emphasize that in making these statements we have been very careful to remain in the commonly defined diffusive regime. The mean free path (defined through the Born approximation) is less than the size of the system. And, with the exception of the width of the IPR distribution, all the properties which are either local in space or "diagonal" in energy are in good agreement with expectations.

The explanation behind these unexpected results is largely open at this time. As briefly discussed in Sec. IV A, one possible scenario would be that the observed statistics are the result of the presence of localized resonances. Further theoretical and numerical work would be needed to prove or disprove this suggestion, but if it held, it would give insight into the transition from the diffusive to localized regime in disordered quantum dots.

In any event, the global off-diagonal quantities that we look at are exactly the quantities that are relevant to electron-electron interactions in finite systems. By looking at the addition energy and ground state spin of our model quantum dots, quantities directly accessible to experiments in the Coulomb blockade regime, we showed that the unexpected statistics have a big effect on observable quantities.

ACKNOWLEDGMENTS

We thank G. Usaj for helpful discussions. This work was supported in part by NSF Grant No. DMR-0103003.

*Permanent address: Laboratoire de Physique Théorique et Modèles Statistiques (LPTMS), 91405 Orsay Cedex, France.

[1] T. V. Ramakrishnan and P. A. Lee, Rev. Mod. Phys. **57**, 287 (1985).
[2] B. L. Altshuler and A. G. Aronov, in *Electron-Electron Interactions in Disordered Systems*, edited by A. L. Efros and M. Pollak (North-Holland, Amsterdam, 1985), pp. 1–153.
[3] I. L. Aleiner, P. W. Brouwer, and L. I. Glazman, Phys. Rep. **358**, 309 (2002), and references therein.
[4] J. von Delft and D. C. Ralph, Phys. Rep. **345**, 62 (2001).
[5] B. L. Altshuler, and B. D. Simons, in *Mesoscopic Quantum Physics*, edited by E. Akkermans, G. Montambaux, J.-L. Pichard and J. Zinn-Justin (North-Holland, Amsterdam, 1995), pp. 1–98.
[6] C. W. J. Beenakker, Rev. Mod. Phys. **69**, 731 (1997).
[7] O. Bohigas, in *Chaos and Quantum Physics*, edited by M. J. Giannoni, A. Voros, and J. Zinn-Justin (North-Holland, Amsterdam, 1991), pp. 87–199.
[8] M. C. Gutzwiller, *Chaos in Classical and Quantum Mechanics* (Springer-Verlag, New York, 1990).
[9] O. Bohigas, M. J. Giannoni, and C. Schmit, Phys. Rev. Lett. **52**, 1 (1984).
[10] S. W. McDonald and A. N. Kaufman, Phys. Rev. A **37**, 3067 (1988).
[11] N. Garcia and A. Z. Genack, Phys. Rev. Lett. **63**, 1678 (1989).
[12] H. Alt, H.-D. Graf, H. L. Harney, R. Hofferbert, H. Lengeler, A. Richter, P. Schardt, and H. A. Weidenmüller, Phys. Rev. Lett. **74**, 62 (1995).
[13] A. Kudrolli, V. Kidambi, and S. Sridhar, Phys. Rev. Lett. **75**, 822 (1995).
[14] K. Müller, B. Mehlig, F. Milde, and M. Schreiber, Phys. Rev. Lett. **78**, 215 (1997).
[15] H.-J. Stöckmann, *Quantum Chaos: An Introduction* (Cambridge University Press, New York, 1999).
[16] T. Guhr, A. Müller-Groeling, and H. A. Weidenmüller, Phys. Rep. **299**, 189 (1998).
[17] P. W. Anderson, Phys. Rev. **109**, 1492 (1958).
[18] N. F. Mott, *Metal-Insulator Transitions* (Taylor & Francis, London, 1990).
[19] B. I. Shklovskii and A. L. Efros, *Electronic Properties of Doped Semiconductors* (Springer-Verlag, New York, 1984).
[20] B. L. Altshuler, V. E. Kravtsov, and I. V. Lerner, in *Mesoscopic Phenomena in Solids*, edited by B. L. Altshuler, P. A. Lee and R. A. Webb (North-Holland, Amsterdam, 1991), pp. 449–521.
[21] A. D. Mirlin, Phys. Rep. **326**, 259 (2000).
[22] J. M. Luttinger, Phys. Rev. **84**, 814 (1951).
[23] A. S. Alexandrov and H. Capellmann, Phys. Rev. Lett. **66**, 365 (1991).
[24] F. Wegner, Z. Phys. B. **36**, 209 (1980).
[25] T. A. Brody, J. Flores, J. B. French, P. A. Mello, A. Pandey, and S. S. M. Wong, Rev. Mod. Phys. **53**, 385 (1981).
[26] V. N. Prigodin and N. Taniguchi, Mod. Phys. Lett B. **10**, 69 (1996), and references therein.
[27] Y. V. Fyodorov and A. D. Mirlin, Phys. Rev. B **51**, 13 403 (1995).
[28] P. Pradhan and S. Sridhar, Phys. Rev. Lett. **85**, 2360 (2000).
[29] M. Schreiber, Phys. Rev. B **31**, R6146 (1985).
[30] J. Bauer, T.-M. Chang, and J. L. Skinner, Phys. Rev. B **42**, 8121 (1990).
[31] F. Evers and A. D. Mirlin, Phys. Rev. Lett. **84**, 3690 (2000).
[32] A. D. Mirlin and F. Evers, Phys. Rev. B **62**, 7920 (2000).
[33] H. U. Baranger, Phys. Rev. B **42**, 11 479 (1990), the discussion of mean free paths is in Appendix C.
[34] C. E. Porter and R. G. Thomas, Phys. Rev. **104**, 483 (1956).
[35] B. Shapiro, Phys. Rev. Lett. **57**, 2168 (1986).
[36] M. V. Berry, J. Phys. A **10**, 2083 (1977).
[37] A. Voros, in *Stochastic Behaviour in Classical and Quantum Hamiltonian Systems*, edited by G. Casati and G. Ford (Springer-Verlag, Berlin, 1979), p. 334.
[38] *Laser Speckle and Related Phenomena*, edited by J. C. Dainty (Spring-Verlag, New York, 1984).
[39] M. Srednicki, Phys. Rev. E **54**, 954 (1996).
[40] V. N. Prigodin, Phys. Rev. Lett. **74**, 1566 (1995).
[41] D. Ullmo and H. U. Baranger, Phys. Rev. B **64**, 245324 (2001).
[42] V. N. Prigodin and B. L. Altshuler, Phys. Rev. Lett. **80**, 1944 (1998).
[43] D. Ullmo, H. U. Baranger, K. Richter, F. von Oppen, and R. A. Jalabert, Phys. Rev. Lett. **80**, 895 (1998).

[44] Y. M. Blanter, Phys. Rev. B **54**, 12 807 (1996).
[45] N. Argaman, Y. Imry, and U. Smilansky, Phys. Rev. B **47**, 4440 (1993), and references therein.
[46] L. P. Kouwenhoven, C. M. Marcus, P. L. McEuen, S. Tarucha, R. M. Westervelt, and N. S. Wingreen, in *Mesoscopic Electron Transport*, edited by L. L. Sohn, G. Schön and L. P. Kouwenhoven (Kluwer, Dordrecht, 1997), pp. 105–214.
[47] G. Usaj and H. U. Baranger, Phys. Rev. B **66**, 155333 (2002), and references therein.
[48] D. H. Cobden and J. Nygård, Phys. Rev. Lett. **89**, 046803 (2002).
[49] Y. Kwon, D. M. Ceperley, and R. M. Martin, Phys. Rev. B **50**, 1684 (1994).